

Journal of Geophysical Research: Solid Earth

RESEARCH ARTICLE

10.1002/2017JB014911

Special Section:

Slow Slip Phenomena and Plate Boundary Processes

Key Points:

- We simulate SSEs in south central Alaska with a nonplanar fault model
- Along-strike variation of effective normal stress controls the segmentation of SSEs
- The segmentation is likely related to the subducted Yakutat Plateau

Supporting Information:

- Supporting Information S1

Correspondence to:

M. Wei,
matt-wei@uri.edu

Citation:

Li, H., Wei, M., Li, D., Liu, Y., Kim, Y., & Zhou, S. (2018). Segmentation of slow slip events in south central Alaska possibly controlled by a subducted oceanic plateau. *Journal of Geophysical Research: Solid Earth*, 123, 418–436.
<https://doi.org/10.1002/2017JB014911>

Received 24 AUG 2017

Accepted 22 DEC 2017

Accepted article online 28 DEC 2017

Published online 15 JAN 2018

Segmentation of Slow Slip Events in South Central Alaska Possibly Controlled by a Subducted Oceanic Plateau

Haotian Li^{1,2} , Meng Wei² , Duo Li³ , Yajing Liu³ , YoungHee Kim⁴, and Shiyong Zhou¹

¹Institute of Theoretical and Applied Geophysics, School of Earth and Space Sciences, Peking University, Beijing, China,

²Graduate School of Oceanography, University of Rhode Island, Narragansett, RI, USA, ³Department of Earth and Planetary Sciences, McGill University, Montréal, Québec, Canada, ⁴School of Earth and Environmental Sciences, Seoul National University, Seoul, South Korea

Abstract Recent GPS observations show that slow slip events in south central Alaska are segmented along strike. Here we review several mechanisms that might contribute to this segmentation and focus on two: along-strike variation of slab geometry and effective normal stress. We then test them by running numerical simulations in the framework of rate-and-state friction with a nonplanar fault geometry. Results show that the segmentation is most likely related to the along-strike variation of the effective normal stress on the fault plane caused by the Yakutat Plateau. The Yakutat Plateau could affect the effective normal stress by either lowering the pore pressure in Upper Cook Inlet due to less fluids release or increasing the normal stress due to the extra buoyancy caused by the subducted Yakutat Plateau. We prefer the latter explanation because it is consistent with the relative amplitudes of the effective normal stress in Upper and Lower Cook Inlet and there is very little along-strike variation in V_p/V_s ratio in the fault zone from receiver function analysis. However, we cannot exclude the possibility that the difference in effective normal stress results from along-strike variation of pore pressure due to the uncertainties in the V_p/V_s estimates. Our work implies that a structural anomaly can have a long-lived effect on the subduction zone slip behavior and might be a driving factor on along-strike segmentation of slow slip events.

1. Introduction

Slow slip events (SSEs) are aseismic slip episodes observed on tectonic faults that do not generate strong seismic signals (Dragert et al., 2001; Peng & Gomberg, 2010; Schwartz & Rokosky, 2007). SSEs are sometimes accompanied by nonvolcanic tremors, and their simultaneous appearance is termed episodic tremor and slip (ETS) (Peng & Gomberg, 2010; Rogers & Dragert, 2003; Schwartz & Rokosky, 2007). SSEs in subduction zones have recurrence intervals of 1–10 years, duration of days to years, and moment magnitudes of 6.0 (detection threshold) to 7.5 (Beroza & Ide, 2011; D. Li & Liu, 2016; Peng & Gomberg, 2010; Saffer & Wallace, 2015; Schwartz & Rokosky, 2007). SSEs tend to occur on the megathrust faults at depths where mechanical and hydraulic properties change significantly in many subduction zones (D. Li & Liu, 2016; Peng & Gomberg, 2010; Saffer & Wallace, 2015). SSEs can be deep (15–70 km) or shallow (0–15 km) (Saffer & Wallace, 2015). The deep SSEs have been linked to high pore pressure near the plate boundaries by seismic observations (Audet & Kim, 2016; Kodaira et al., 2004) and numerical simulations (Colella et al., 2012; Y. Liu & Rice, 2007; Matsuzawa et al., 2010). The shallow SSEs have been linked to highly overpressured fluid and the subduction of rough seafloor (Saffer & Wallace, 2015).

The characteristics of SSEs also change along strike in many subduction margins around the world (Brudzinski & Allen, 2007; Wallace & Beavan, 2010), but reasons for this along-strike segmentation are not fully understood. For deep SSEs, the possible causes include along-strike variations of pore pressure related to silica enrichment (Audet & Bürgmann, 2014), strength variation of upper geological terranes from composition change (Brudzinski & Allen, 2007), variations of effective normal stress (Y. Liu, 2014; Watkins et al., 2015), and slab geometry (D. Li & Liu, 2016). For the shallow SSEs, it is suggested that pore pressure, geometrical, and compositional heterogeneity might be the main cause (Saffer & Wallace, 2015). It is also possible that multiple mechanisms are at play in individual subduction zones.

In this paper, we focus on the along-strike segmentation of deep SSEs in south central Alaska. The established GPS and seismic network in Alaska and the observations of SSEs in south central Alaska, as described in detail

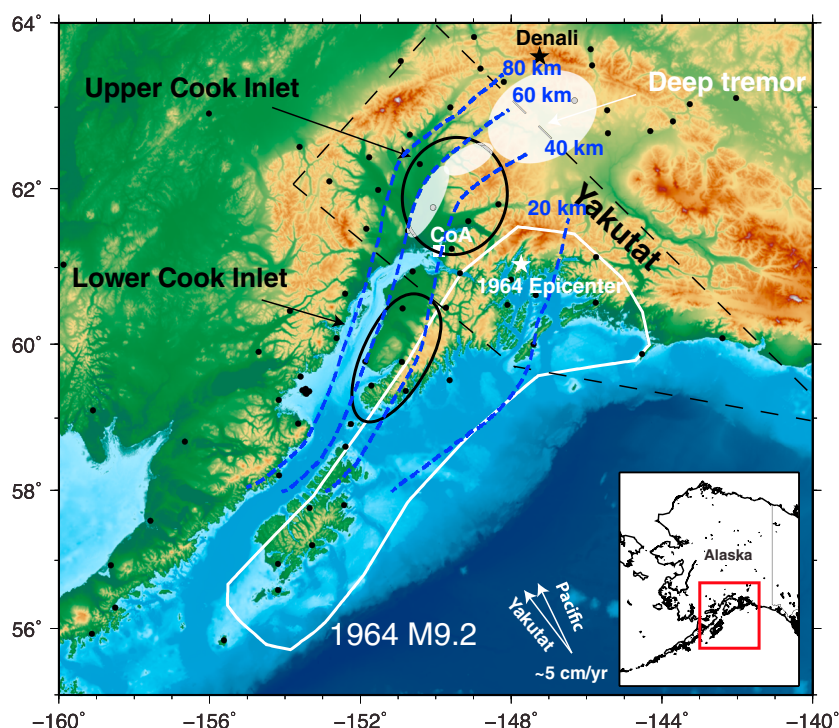


Figure 1. Map of south central Alaska, including the epicenter (white star) and the rupture area (white solid line region) of the 1964 M_w 9.2 earthquake (Furumoto, 1965; Plafker, 1965), two SSE patches (black ellipses) (Fu et al., 2015; S. Li et al., 2016; Wei et al., 2012), estimated boundaries of the subducted Yakutat Plateau (black dashed line) (Eberhart-Phillips et al., 2006), and deep tremor (white ellipses) (Wech, 2016). The blue dashed lines indicate the contours of the plate interface depth from J. Li et al. (2013). The white arrows that show the plate motion for Pacific and Yakutat slabs are also shown (J. Li et al., 2013). The black star shows the epicenter of the 2002 M_w 7.8 Denali earthquake, the white star shows the epicenter of the 1964 M_w 9.2 Alaska earthquake, and the white square is the city of Anchorage (CoA).

in section 2 below, offer a unique opportunity to identify the mechanism of along-strike SSE segmentation in this region. Between 1995 and 2017, at least two repeating SSE episodes have been identified in both Upper and Lower Cook Inlet with distinctive duration, interval, magnitude, and spatial extent, suggesting that the SSEs in south central Alaska may be segmented (Figures 1 and 2 and Table S1 in the supporting information). Here we first summarize the tectonic setting and seismic/geodetic observations and review some possible mechanisms of SSE segmentation in this region. We then focus on two most plausible mechanisms: (1) the variation of slab geometry and (2) the variation of effective normal stress at the SSE depths—is responsible for the SSE segmentation in south central Alaska. We further test these hypotheses using numerical modeling of SSEs in the framework of rate-and-state friction.

2. Tectonic Setting and Observations of SSEs and Tremors in South Central Alaska

The active subduction of the Pacific Plate beneath Alaska dominates the tectonics of south central Alaska (J. Li et al., 2013; Nokleberg et al., 2000; Plafker & Berg, 1994), with the eastern termination of the subduction coincident with the subducted Yakutat Plateau (Eberhart-Phillips et al., 2006; Nokleberg et al., 2000; Plafker & Berg, 1994). One of the world's largest SSEs has occurred in this region, with an equivalent moment magnitude M_w of 7.5 (Fu et al., 2015). The 1964 M_w 9.2 megathrust earthquake, which is the second largest earthquake ever recorded instrumentally (Lay, 2015), also occurred here (Furumoto, 1965; Plafker, 1965) (Figure 1).

Recent GPS measurements have identified two pairs of repeating SSEs that abut the downdip end of the 1964 megathrust rupture area (Figures 1 and 2 and Table S1) (Fu et al., 2015; S. Li et al., 2016; Wei et al., 2012). In Upper Cook Inlet near the city of Anchorage, the SSEs have an equivalent moment magnitude of 7.2–7.5 and ruptured the same area during the two episodes in 1998–2001 (Ohta et al., 2006) and 2009–2013 (Fu et al., 2015), resulting in an average duration of 3–4 years and an interval of about 11 years. Farther

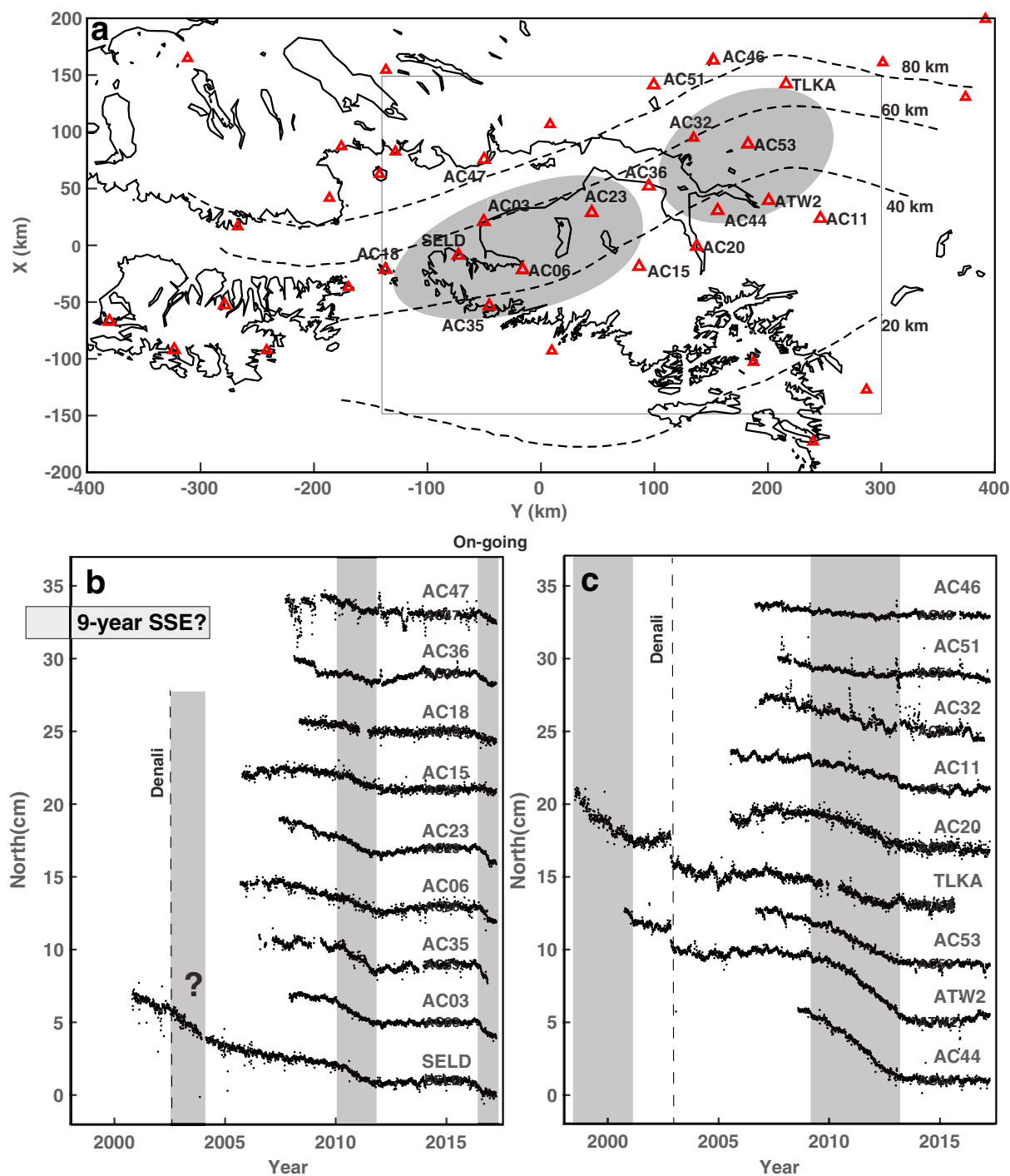


Figure 2. Segmentation of SSEs in south central Alaska into two distinct regions. (a) Map of the south central Alaska in Cartesian coordinates. The red triangles are PBO GPS stations. Shaded ellipses highlight the two SSE patches. The dashed lines are the depth contour of the slab. The rectangle shows the simulation area. (b) North component of GPS daily solutions for selected stations after removing linear trends from the time series in the pink area. The data were referred to igs08 frame and were downloaded from UNAVCO ftp on 19 April 2017. The vertical gray rectangles highlight the SSEs. The dashed line shows the time of M_w 7.9 Denali earthquake in 2008. The horizontal light gray rectangle highlights the 9 year SSE proposed by S. Li et al. (2016). (c) North component of GPS daily solutions for selected stations after removing linear trends from the time series in the blue area. The vertical gray rectangles highlight the SSEs.

southwest in Lower Cook Inlet, a SSE with a moment magnitude of 6.9 occurred between 2010 and 2012 (Wei et al., 2012). A similar SSE likely occurred between 2003 and 2005 based on a continuous GPS station installed in October 2000 but was interpreted to be part of a longer episode from at least 1995 to 2004 based on campaign GPS data (S. Li et al., 2016). We suspect that there was a change of SSE behavior around 2002 in

Lower Cook Inlet and will discuss its implication in more detail in section 6. Another SSE with a similar magnitude and spatial extent to the 2010–2012 episode started in early 2016 and is still ongoing (Figure 2). Thus, it is clear that the SSEs in Lower Cook Inlet since 2002 have different characteristics from those in Upper Cook Inlet. These different duration, magnitude, and spatial extent suggest that there are two distinct segments of SSEs in south central Alaska.

The interval, duration, magnitude, and spatial extent of SSEs in any given subduction zone do vary from episode to episode on any given segment, but the average value over many episodes does provide characteristic quantities that can be used to estimate the physical conditions on the fault zone, as best illustrated in Cascadia (Brudzinski & Allen, 2007; Schmidt & Gao, 2010), southwest Japan (Hirose & Obara, 2010), Costa Rica (Dixon et al., 2014), and New Zealand (Wallace & Beavan, 2010). Because only two to three SSE episodes have been observed in either Upper or Lower Cook Inlet in south central Alaska, it is unclear whether the segment boundary between Upper and Lower Cook Inlet is permanent over many episodes or will change over time. However, there are several pieces of evidence suggesting that the physical condition of the two segments is different. First, SSEs in Upper Cook Inlet occurred on the subducted Yakutat Plateau, whereas the SSEs in Lower Cook Inlet happened over a normal oceanic crust (Figure 1). The geological terrain boundary appears to coincide with the segmentation boundary between the two SSE slip patches (Figure 1). Second, tremor activities are also segmented the same way as SSEs (Wech, 2016). No tremor has been observed in Lower Cook Inlet, whereas tremors occurred episodically with an interval of 3–6 months in Upper Cook Inlet without a clear temporal correlation to the SSEs (Figure 1) (Wech, 2016). These tremors are at the downdip end of the 1998–2001 slow slip patch but have a significant overlap with the slip area of the 2009–2013 event (Fu & Freymueller, 2013; Peterson & Christensen, 2009; Wech, 2016). Therefore, the along-strike segmentation of SSEs in this region is probably robust.

3. Review of Candidate Mechanisms of SSE Segmentation

3.1. Along-Strike Variation of Pore Pressure Related to Silica Enrichment

Low V_p/V_s ratios near the subduction interface have been observed at depths of slow slip events, suggesting high pore pressure in SSE source region (Audet & Kim, 2016; Kodaira et al., 2004). Audet and Bürgmann (2014) compiled seismic data at several subduction zones and found that the average SSE recurrence interval is linearly correlated with the average V_p/V_s ratio in the overlying forearc crust but uncorrelated with that in the low-velocity zone (LVZ, interpreted as saturated upper oceanic crust), although the V_p/V_s ratio in the LVZ is much higher (~2.4–2.8) than that in the forearc crust (~1.6–2.0). They suggest that different levels of silicate enrichment in the forearc crust are responsible for the V_p/V_s ratio variation. The three segments, from south to north, Klamath, Siletzia, and Wrangellia, along the Cascadia margin also fit this linear correlation, suggesting that the along-strike segmentation of SSEs in Cascadia is linked to the pore pressure heterogeneity caused by silica enrichment (Audet & Bürgmann, 2014).

Here we estimated the V_p/V_s ratio in the forearc crust from seismic data using the grid search stacking method of the receiver functions (Zhu & Kanamori, 2000) with a fixed V_p of 6.3 km/s for the forearc crust. Because there is a thick basin in this region, we selected 11 stations that show clear seismic signals and are less influenced by the basin structure (Figure 3a). We found that the V_p/V_s ratios at updip stations (BLAK and MAIN) are slightly higher than that the nine stations above the SSE zone (average value of 2.0 versus 1.8), although the error bars do overlap (Figure 3b). We did not find any significant along-strike variation in the V_p/V_s ratio in the forearc crust at the stations above the slow slip source region (Figure 3b). Although the V_p/V_s ratio is comparable to values for other subduction zones (~1.6 to 2.0), the much longer SSE recurrence intervals (~8 to 11 years) clearly position south central Alaska off the linear correlation established by Audet and Bürgmann (2014), which indicates that the “silica enrichment” mechanism may not be as effective in Alaska, possibly related to subduction of the relatively old, cold Pacific Plate and hence peak metamorphic dehydration is farther downdip from the SSE zone (Wada & Wang, 2009).

We also estimated the V_p/V_s ratio in the low-velocity zone (LVZ) from seismic data using the receiver-function waveform modeling method (Kim et al., 2014), exploring evidence for along-strike variation of fluid and pore pressure in the subduction zone. We constructed 1-D velocity models for the 11 seismic stations above the thrust zone, which fit arrival times and amplitudes of the primary converted phase at the top and bottom

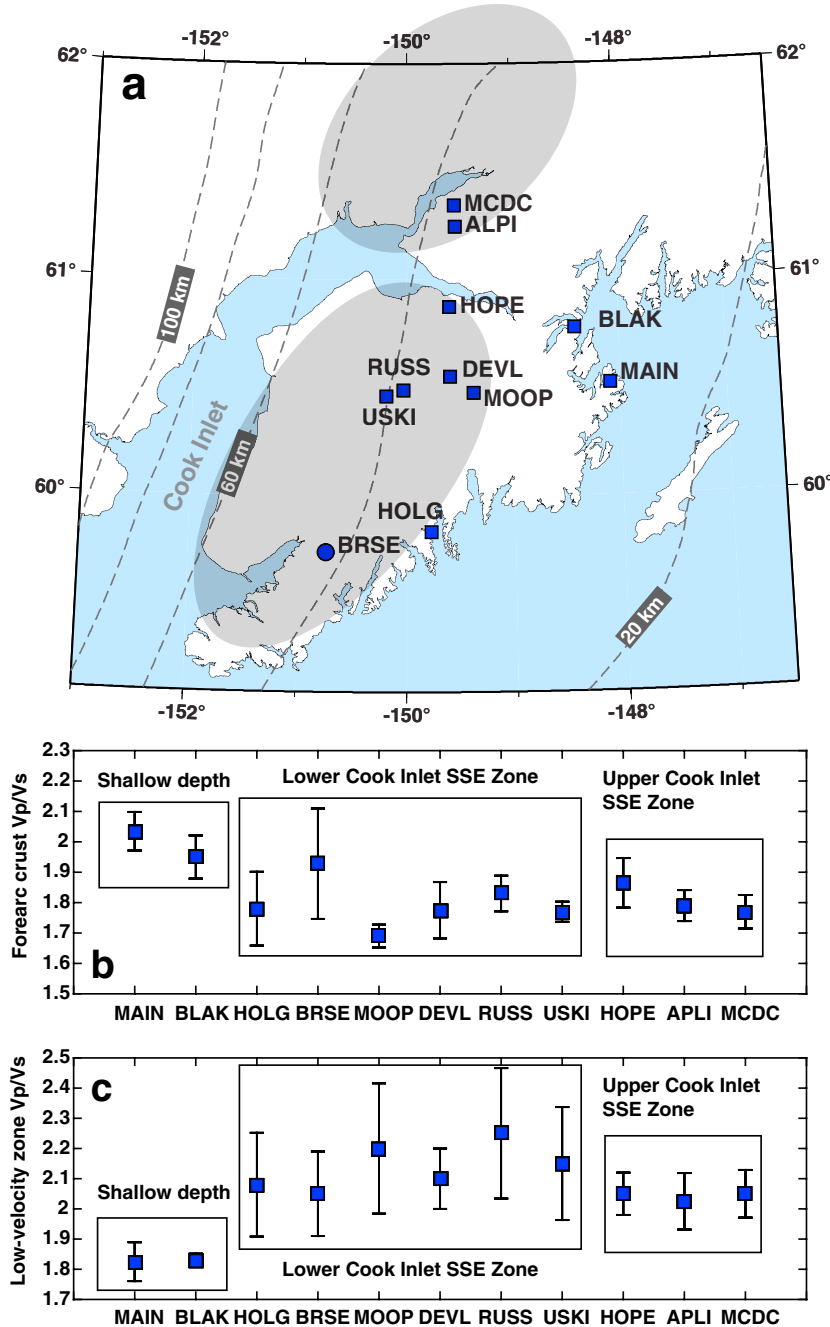


Figure 3. (a) Map of the study area. The blue rectangles and circle are seismic stations from MOOS and AEIC network, respectively. Dashed lines are depth contour from J. Li et al. (2013). The gray area highlights the SSE zones. (b) The V_p/V_s ratio in the forearc crust. The blue squares are the average value, and the black bars show the 95% uncertainty. (c) The V_p/V_s ratio in the low-velocity zone. The blue squares are the average value, and the black bars show the 95% uncertainty.

of the thrust layer as well as those of the free-surface multiples of the thrust layer. We fixed the thickness of the LVZ layer as 2.0 km. We iteratively determined a range of V_p/V_s values for the LVZ layer by minimizing the misfit between the synthetic and observed receiver functions. We found that the V_p/V_s ratios at stations above the SSE zones are above 2.0 and, despite their large uncertainties, are systematically higher than the ratios of ~1.8 measured at updip stations (BLAK and MAIN), even though the error bars do overlap (Figure 3c). Similar to the forearc crust, we did not find much along-strike change in the V_p/V_s ratio in the LVZ layer (Figure 3c), suggesting that there is no significant contrast in pore pressure between the Lower

and Upper Cook Inlet SSE zones. However, we could not exclude the possibility of along-strike variation in pore pressure at the level of tens of megapascals because of the uncertainties in V_p/V_s estimation for those stations.

3.2. Compositional Changes of the Upper Geological Terrane

Brudzinski and Allen (2007) reviewed the segmentation of ETS in Cascadia and found the average recurrence interval is inversely proportional to the upper plate topography and the spatial extent correlates with geologic terranes. The largest ETS zone in Cascadia is immediately landward from a paleoseismic asperity (Goldfinger et al., 2008; Song & Simons, 2003; Wells et al., 2003), and marine sediments studies in the forearc basins also indicate that offshore paleoseismic “patches” could affect the along-strike segmentation of tremors in Cascadia (Boyarko et al., 2015). In other words, there is a spatial link between the subduction zone earthquake and ETS. It is not yet clear if any temporal link exists, but the intervals between ETS episodes could be controlled by strength variations, reflected as loading conditions on the megathrust fault, due to the composition of geologic terranes. In Alaska, seismic asperities are just seaward from the Upper and Lower Cook Inlet SSE segments (Ichinose et al., 2007) and the spatial link between megathrust earthquake and SSEs is likely. However, there is no significant along-strike change in the geological terranes or the upper plate topography in Cook Inlet (Plafker & Berg, 1994).

As D. Li and Liu (2017) suggested, gravity anomalies, which reflect the along-strike variation of the overlying lithosphere, can be used to constrain the along-strike variation of effective normal stress. Isostatic residual gravity data spanning Alaska are available (Barnes et al., 1994; Saltus et al., 1999). The gravity data in the study region are dominated by gravity lows (-80 mGal) in the surficial basin along the entire Cook Inlet, and the gravity anomaly in both SSE regions is near zero (Barnes et al., 1994). Therefore, there is little correlation between the gravity anomaly and the SSE segmentation in this region.

3.3. Slab Geometry

Fault geometry has long been recognized to affect seismic and aseismic slip on a fault. Mitsui and Hirahara (2006) demonstrated in a conceptual model with three planar elements that SSE generation is sensitive to varying fault dip angles. Matsuzawa et al. (2013) found that shallower-dipping faults can lead to large SSEs, which is consistent with geodetic observations in Shikoku (Kobayashi, 2010, 2012). Recently, D. Li and Liu (2016) incorporated the realistic fault geometry of northern Cascadia in the framework of rate-and-state friction to simulate the spatiotemporal evolution of SSEs on a nonplanar subduction fault. They found that the along-strike segmentation of SSEs is inversely related to the local fault dip and strike angles of the slow slip zone, suggesting strong geometrical control on the slow slip process in Cascadia (D. Li & Liu, 2016).

The SSEs in south central Alaska are in general consistent with this model. The dip angle of the slab between 40 and 60 km (SSE depth range) in Upper Cook Inlet is $\sim 16^\circ$, slightly higher than an average dip angle of $\sim 13^\circ$ in Lower Cook Inlet (Figure 1) (J. Li et al., 2013), because the buoyant, thickened Yakutat crust can sustain shallow slab dip (Abers, 2008). The average along-dip width between 40 and 60 km depth in Upper Cook Inlet is 58.8 km and that in Lower Cook Inlet is 53.5 km. It is possible that the along-strike variation of slab geometry contribute to the SSE segmentation, although the variation is small compared to what D. Li and Liu (2016) investigated for northern Cascadia. This is the first hypothesis that we will test in section 4.

3.4. Existence of the Yakutat Plateau

The boundary between the two SSE segments in south central Alaska aligns well with the western boundary of the Yakutat Plateau (Figures 1 and 2). This suggests that the partitioning and variation of the two SSE segments might be related to the subduction of the oceanic plateau. This connection has been noticed by many previous studies. For example, Wech (2016) studied tremors in this region and suggested that the Yakutat Plateau controls the segmentation of tremors in this region. Ohta et al. (2006) and Fu and Freymueller (2013) noticed that the western edge of SSEs in Upper Cook Inlet is close to the western edge of the Yakutat Plateau.

One way that the Yakutat Plateau could cause the segmentation is by locally decreasing the negative buoyancy available to drive subduction and hence produce a higher effective normal stress due to the presence of a thicker crust (Arrial & Billen, 2013). The magnitude of the extra buoyancy depends on the thickness and the lateral dimension of the subducted plateau as well as the depth of basalt to eclogite transition, which

substantially increases the density of the oceanic crust. In south central Alaska, the eclogitization depth is estimated to be around 120 km (Rondenay et al., 2008) and thus has negligible effect on the plateau density within the SSE depth range. According to seismic reflection and refraction data, offshore the thickness of the Yakutat Plateau increases west to east from ~15 km to ~30 km and is much thicker than normal oceanic crust (Christeson et al., 2010; Worthington et al., 2012). Taking the typical density of oceanic crust and mantle (3.0 versus 3.3 g/cm³), an extra 5 km of material would result in about 15 MPa of positive buoyancy or equivalently a 15 MPa increase in effective normal stress.

Another mechanism that the presence of the Yakutat Plateau could contribute to the SSE along-strike segmentation is by releasing different amounts of fluids and therefore leading to a contrast in pore pressure in the fault zone. On one hand, Chuang et al. (2017) proposed that significant amounts of fluids of the Yakutat Plate has been released from its upper crust during subduction and creates hydromechanical conditions similar to those in warm subduction zones favorable for nontectonic tremors. This model can explain the occurrence of tremors in the Denali volcanic gap. However, the available fluid source does not necessarily lead to high pore pressure. A permeability “seal” or other mechanisms for retaining fluids along the subduction interface is required to profoundly raise the pore pressure level. A seismic profile east of Prince William Sound and other data suggested the entire sedimentary cover on top of the Yakutat Plateau was scraped off in the subduction process (Worthington et al., 2012). The same process could happen for the Yakutat Plateau under Upper Cook Inlet. If true, there will be no seal for retaining fluid. Due to the difficulty to quantify the along-strike contrast in fault zone pore pressure, we couple its effect with fault normal loading and together modeled as the effective normal stress (normal stress minus pore pressure).

3.5. Summary of Candidate Mechanisms

Based on the above discussion, we will focus our analysis on two mechanisms: (1) the along-strike variation of slab geometry and (2) along-strike variation of effective normal stress caused by the subduction of the Yakutat Plateau. Next, we will test the two hypotheses by simulating SSEs in south central Alaska in the framework of rate-and-state friction with a nonplanar fault.

4. Numerical Model

We run numerical simulations in the framework of rate-and-state friction to understand the mechanism that controls the SSE segmentation in south central Alaska. On one hand, SSEs occur at the depth where the mechanical properties of rock transition from brittle to ductile. Other mechanisms have been proposed to explain the generation of nonvolcanic tremors and SSEs, such as semibrittle fracture growth (Reber et al., 2015), dehydration-induced porosity waves (Skarbek & Rempel, 2016), and a thermorheological model (X. Gao & Wang, 2017). On the other hand, SSEs are usually accompanied by nonvolcanic tremors and low-frequency earthquakes (LFEs) (Obara, 2002; Rogers & Dragert, 2003; Shelly et al., 2006, 2007). The LFEs are due to shear faulting on the subduction zone plate interface, suggesting that tremors, LFEs, and SSEs are different manifestations of a single process (Shelly et al., 2006, 2007). Therefore, it is reasonable to model SSEs as frictional sliding on the plate interface (Y. Liu & Rice, 2005, 2007).

Based on variants of rate-and-state friction models, there are mainly three kinds of frictional-sliding simulations of SSEs. The first kind uses the “standard” rate-and-state friction model, where SSEs nucleate in the velocity-weakening (potentially unstable) region near the transition to velocity-strengthening (stable) behavior (Colella et al., 2012; Y. Liu & Rice, 2005, 2007, 2009; Rubin, 2008; Watkins et al., 2015). The second kind couples the shear-induced dilatancy strengthening with the velocity-weakening friction (Y. Liu, 2013; Y. Liu & Rubin, 2010; Segall et al., 2010; Segall & Rice, 1995). The last kind uses a frictional law that is velocity weakening at low slip speeds but velocity strengthening at high speeds, termed a cutoff velocity model (Hawthorne & Rubin, 2013a, 2013b; Matsuzawa et al., 2013; Okubo, 1989; Shibasaki & Shimamoto, 2007; Weeks, 1993). With proper parameter tuning, all three kinds of models can reproduce the major SSEs characteristics, including recurrence interval, magnitude, and duration. Here we use a standard rate-and-state friction model as described in section 4.2.

Most previous simulations of the source physics of SSEs are performed on a planar fault discretized by rectangular elements for the sake of simplicity and low computational cost (Colella et al., 2012; Y. Liu & Rice, 2007; Matsuzawa et al., 2010). In this study, we adopt a triangular dislocation element approach (D. Li & Liu, 2016;

Matsuzawa et al., 2013), which allows us to simulate SSE processes on a nonplanar and more realistic fault geometry and test the hypothesis that slab geometry caused the segmentation.

4.1. Fault Geometry and Computation Domain

Over the past 35 years, earthquake locations have been used to delineate the geometry of the subducting plate in Alaska (Brocher et al., 1994; Doser & Veilleux, 2009; Page et al., 1989; Pulpan & Frohlich, 1985; Ratchkovski & Hansen, 2002; Stephens et al., 1984; Van Wormer et al., 1974). The latest of these efforts is presented by the Slab 1.0 model (Hayes et al., 2012), and J. Li et al. (2013). Slab 1.0 is a widely used compilation of three-dimensional slab geometry of major subduction zones. However, Slab 1.0 is clearly too deep in our study area because the interface in the model is below the slab earthquakes. J. Li et al. (2013) used data from the MOOS (Multidisciplinary Observations Of Subduction) project, which deployed a dense temporary seismic network on the Kenai Peninsula in 2006–2009. They used an automatic algorithm to detect earthquakes during the deployment and conducted a joint inversion for hypocenters and velocity structure. They then relocated these earthquakes by double difference (hypoDD) (Waldauser & Ellsworth, 2000). These micro-earthquakes delineate the geometry of Alaska subduction plate. According to this model, the dip angle of the slab between 40 and 60 km depth in Upper Cook Inlet is ~16°, slightly higher than ~13° in Lower Cook Inlet. We use the updated slab geometry from J. Li et al. (2013) in our simulation.

Our study area encompasses the region extending from longitude 142°W to 158°W and latitude 55°N to 64°N that contains the two SSE segments. To simplify the computation, we transformed our research area using a 50° clockwise rotation with respect to an origin at (151°W, 60°N). In this new Cartesian coordinate system, the x axis aligns with the along-strike direction, and the y axis aligns with the downdip projection of the subducting slab (Figure 2a). The z axis represents depth. Our chosen study region spans x values from –150 to 300 km and y values from –150 to 150 km. We discretized this 450 × 300 km area into 31,909 2 × 2 km square cells, divided each cell into two congruent triangles, and projected the triangular grids onto the 3-D subduction fault surface. We also tested a 1 km cell size and found that the 2 km size model gave the same SSE cycles but took much less computation time.

4.2. Governing Equations

We simulated Alaska SSEs in the framework of rate-and-state friction (Y. Liu & Rice, 2007; Scholz, 1998; Wei et al., 2013). The evolution of fault shear stress τ (Dieterich, 1979; Ruina, 1983) is as follows:

$$\tau = \bar{\sigma}f = (\sigma - p) \left[f_0 + a \ln\left(\frac{V}{V_0}\right) + b \ln\left(\frac{V_0\theta}{D_c}\right) \right]. \quad (1)$$

The friction coefficient f is dependent on the fault slip rate V and the state variable θ , which represents memory of slip. Here a and b are nondimensional rate-and-state friction parameters, D_c is the characteristic distance, f_0 is the friction coefficient at a reference velocity V_0 at steady state, and $\bar{\sigma} = (\sigma - p)$ is the effective normal stress, where σ is the normal stress, and p is the pore pressure. We used the “aging” law, which is one of the most commonly used evolution laws that allows friction to evolve on stationary asperity contacts, as supported by laboratory experiments (Beeler et al., 1996):

$$\frac{d\theta}{dt} = 1 - \frac{V\theta}{D_c}. \quad (2)$$

Another widely used law to describe the evolution of the state variable is the “slip” law, which requires non-zero slip for friction evolution and has been shown to better represent slip during earthquake nucleation, especially at a large-velocity step and a narrower range of suitable conditions for slow slip (Ampuero & Rubin, 2008). Simulations with the same set of codes on Cascadia SSEs using both the slip law and the aging law show that the aging law allows more flexibility in the choice of parameters (D. Li & Liu, 2017). Therefore, we used the aging law here.

We adopt the quasi-dynamic relation between shear stress and fault slip following Rice (1993):

$$\tau_i(t) = - \sum_{j=1}^N K_{ij} (\delta_j(t) - V_{pl} t) - \eta \frac{d\delta_i(t)}{dt}, \quad (3)$$

where $\tau_i(t)$ and $\delta_i(t)$ are shear stress and slip on element i , respectively, and the stiffness matrix K_{ij} represents the shear stress change on element i due to a unit dislocation in the dip direction on element j . This Green’s

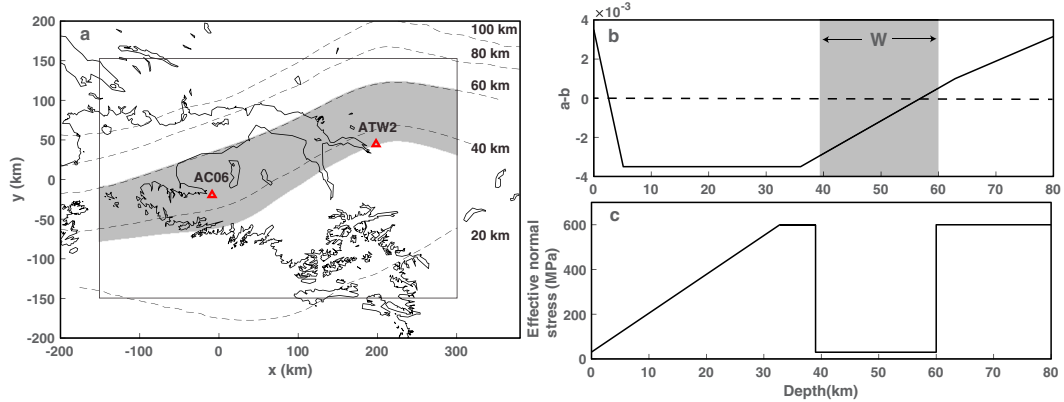


Figure 4. (a) Map of south central Alaska. The black dashed lines are the depth contour. The gray area is the depth range of low effective normal stress, 39–60 km. The black solid box shows the simulation area. The two red triangles are GPS stations. (b) The relationship between $a-b$ and depth based on the observed slip region of SSEs and the slab geometry model (J. Li et al., 2013). The gray area is the low effective normal stress region. (c) Effective normal stress used in the simulations. We varied the effective normal stress in the 39–60 km depth range in simulations but keep it constant at 600 MPa outside the zone. Distribution of D_c is set to a constant at 10 mm between 39 and 60 km depth and 2,000 mm outside.

function K_{ij} is calculated in an elastic half-space medium (Okada, 1992), as first implemented for triangular dislocation elements by Stuart et al. (1997) and benchmarked here against a MATLAB code developed by Meade (2007). The radiation damping factor $\eta = \frac{\mu}{2c_s}$ (μ is elastic shear modulus, and c_s is shear wave speed) is introduced to prevent the slip velocity from going unbounded during an earthquake (Rice, 1993). This quasi-dynamic approach can be considered to be appropriate for simulating slow slip processes with the updip seismogenic zone fully locked (Y. Liu & Rice, 2007, 2009).

4.3. Key Parameters

The key parameters in our simulation are listed in Table S2 and shown in Figure 4. Although the convergence rate gradually increases toward the west along the Alaskan-Aleutian arc, it is about 55 mm/yr with little variation in our simulation region (Cohen & Freymueller, 2004). We set the shear modulus $\mu = 50$ GPa (Suito & Freymueller, 2009) and the Poisson's ratio $\nu = 0.25$. We define the onset of an SSE as the time when the maximum velocity on the fault reaches 3 times the plate convergence rate, which is close to the GPS detection threshold in this region.

In the rate-and-state framework, the friction parameter $a-b$ determines if the fault segment deforms during stick-slip events (earthquakes or SSEs) or via continuous creep (not an earthquake). When $a-b$ is positive (velocity strengthening, VS), the fault slips continuously and aseismically, a scenario called creep. When $a-b$ is negative (velocity weakening, VW), slip can be either unstable or conditionally stable, depending on a nondimensional parameter W/h^* , where W is the along-dip width of the VW zone (Figure 4) and $h^* = \frac{2\mu b D_c}{\pi(b-a)^2 \bar{\sigma}}$ is the minimum fault size for unstable fault slip, referred to as a characteristic nucleation size (Rubin & Ampuero, 2005). The length ratio W/h^* has been found to be a key parameter in determining the occurrence of aseismic versus seismic slip events in subduction zones and transform faults (Y. Liu et al., 2012; Y. Liu & Rice, 2007; Wei et al., 2013). For a large effective normal stress $\bar{\sigma}$ or a large VW zone where W/h^* is larger than 1.0, fault slip is seismic. In contrast, when W/h^* is between 0.6 and 1.0, the fault slip as an SSE, and below this narrow W/h^* range, the fault motion can only be continuous creep (Y. Liu & Rice, 2005, 2007). In other words, the width of the low-effective-normal-stress zone needs to be large enough that unstable slide can nucleate but not too large that the event becomes seismic (Rubin, 2008). So once other parameters are set, the choice of D_c (therefore nucleation size h^*) will determine the behavior of the system.

In laboratory rock-sliding experiments, the friction stability parameter $a-b$ depends on temperature, rock type, and loading conditions (Blanpied et al., 1998). Usually, a thermal model of the fault is used to convert laboratory-measured temperature-dependent $a-b$ into depth-dependent distribution on the fault. The depth at which $a-b$ equals zero defines the transition from seismic to aseismic slip, that is,

downdip range of SSEs, such as in Cascadia (Y. Liu & Rice, 2007). The stability transition isotherm is about 350°C for wet granite gouge (Blanpied et al., 1998) and about 500°C for wet gabbro gouge under supercritical water conditions (He et al., 2006). However, the subducting slab is much colder in Alaska than in Cascadia, and the 350° isotherm would be at about 80 km (Syracuse et al., 2010), a depth much deeper than the maximum depth of the observed SSEs. Thus, the downdip limit of SSEs in south central Alaska is more likely related to the depth of the continental Moho (X. Gao & Wang, 2017; Hyndman, 2013), or alternatively, rocks at these depths may no longer be primarily composed of granite or gabbro. An example of the distribution of $a-b$ in our model is shown in Figure 4b. The lower stability transition of $a-b$ is set to be close to 60 km depth, to be consistent with GPS observations of the slip area of SSEs. The exact values of parameter $a-b$ do not strictly reflect a particular type of rocks measured from laboratory experiments. Rather, we allowed $a-b$ to vary in order to fit GPS observations but kept them in the same order of magnitude (i.e., ~0.001) as from laboratory measurements.

Low effective normal stress due to elevated pore pressure, as supported by results from teleseismic receiver functions in this region (Kim et al., 2014), is necessary for generating episodic SSEs. In our simulation, the low effective normal stress zone is confined to a depth range between 39 and 60 km (Figure 4), to be consistent with GPS observations of SSE slip area. The continental Moho depth in south central Alaska near the shore is about 35–45 km and likely increases inland (Christeson et al., 2013; Veenstra et al., 2006). Dehydration from minerals near the continental Moho likely provides the fluids and gives rise to the occurrence of SSEs and tremor (X. Gao & Wang, 2017; Hyndman, 2013). We set the stress above 39 km to be linearly increase with depth until reaching 600 MPa, effectively locking the fault above 39 km depth, as we are most interested in the SSE behavior between large earthquakes. We set the stress below 60 km also to be 600 MPa to prevent SSEs from propagating farther downdip. We set D_c above 39 km and below 60 km to be 2,000 mm for the same rational. We tested stress in the range of 10–35 MPa and D_c in the range of 10–30 mm between 39 and 60 km to match GPS observations of SSE duration and recurrence time.

5. Model Results

We conducted a systematical parameter search, designed in two sets of simulations, aiming to test two mechanisms that control the SSE segmentation in this region: along-strike variation of (1) slab geometry and (2) effective normal stress. We tried to reproduce the SSE observations, including the along-strike segmentation and the average interval and duration of SSEs. In Upper Cook Inlet, large SSEs with duration of 3–4 years repeat about every 11 years. In Lower Cook Inlet, moderate SSEs with duration of 2 years repeat about every 7 years, at least for events since 2002. We note that the SSE behavior in Lower Cook Inlet before 2002 is more complicated and may not follow the post-2002 pattern. We will discuss this in detail in section 6.

First, we run a set of simulations without along-strike variation of parameters except the geometry to test hypothesis one. We varied one parameter at a time, including the convergence rate V_{pl} , $a-b$, D_c and the effective normal stress $\bar{\sigma}$, in the plausible ranges as documented in laboratory experiments and/or supported by seismological observations. We did not vary h^* separately as D_c and h^* are dependent once other parameters are set.

Second, we run a set of simulations where we allowed key parameters (effective normal stress $\bar{\sigma}$) to change along strike. As will be shown later, the contrast of effective normal stress can reproduce the observed along-strike segmentation of SSEs.

5.1. Testing Hypothesis One: Fault Geometry

The main effect on numerical simulations of a nonplanar fault geometry is the along-strike variation of W , the along-dip width of the SSE region. As discussed earlier, the length ratio W/h^* is a key parameter in determining the occurrence of aseismic versus seismic slip events in subduction zones and transform faults (Y. Liu et al., 2012; Y. Liu & Rice, 2007; Wei et al., 2013). For a fault of an elongated shape, W/h^* also determines if the SSEs are segmented (Y. Liu, 2014). In most simulations of this type, h^* is fixed, so W becomes the only parameter to determine SSEs behavior. To understand the influence of geometry on the spatial and temporal evolution of SSEs, we used a planar subduction fault model with a dip angle of 12° and a nonplanar subduction fault model (J. Li et al., 2013). Figure 5 shows the evolution of slip velocity, averaged over W , for the planar

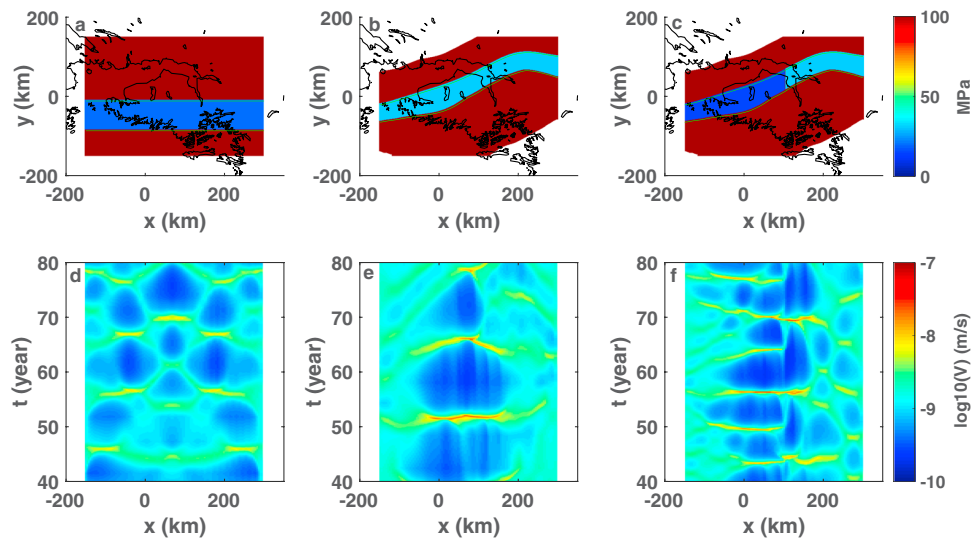


Figure 5. Models with different slab geometry and effective normal stress and the SSE behavior. (a) The effective normal stress distribution of the planar model. The effective normal stress is 15 MPa in the low effective normal stress zone and 600 MPa elsewhere. (b) The effective normal stress distribution of the J. Li et al. (2013) Model, 30 MPa in the blue zone and 600 MPa elsewhere. (c) The effective normal stress distribution of the Li model with along-strike variation, 15/30 MPa in the blue zone and 600 MPa elsewhere. The average slip velocity in the depth of low effective normal stress and velocity-weakening zone change over time of (d) planar model, (e) J. Li et al. (2013), model and (f) J. Li et al. (2013) model with different effective normal stress in the west and east. Red/yellow colors represent SSEs. The nucleation size D_c is set to be 10 mm between 39 and 60 km depth and 2,000 mm outside for all simulations.

and nonplanar fault models. For the planar fault model (Figures 5a and 5d), SSEs are segmented, and SSEs do not rupture the entire fault. Y. Liu (2014) also observed this phenomenon on a planar fault model set up for Cascadia. However, the SSE repeating interval of different segments as shown in Figures 5a and 5d is similar, which is inconsistent with GPS observations. The SSEs generated in the nonplanar fault with same $\bar{\sigma}$ along strike ruptured the entire fault and does not show segmentation (Figures 5b and 5e). Therefore, the geometry might play a negligible role in SSE segmentation in south central Alaska. As explained in more detail next, the along-strike variation of $\bar{\sigma}$ could reproduce the observed segmentation (Figures 5c and 5f).

To understand how key SSE characteristics (interval, duration, and amplitude) change with parameters, we run a series of simulations without along-strike variation other than geometry. We calculated synthetic surface deformation at GPS stations AC06 (Lower Cook Inlet) and ATW2 (Upper Cook Inlet), to represent the two SSE patches. We started with a reference model then varied one parameter at a time. The results are shown in Figure 6 and Table S3. First, the trend of change at the two stations is similar. The amplitude of SSEs at ATW2 is bigger than that at AC06, whereas interval and duration are similar, likely because station ATW2 is closer to the center of SSEs. Second, key characteristics are very sensitive to the effective normal stress, less sensitive to convergence rate and $a-b$, and not very sensitive to D_c at the range we tested. To make the interval longer, one may increase the effective normal stress, decrease the convergence rate, or decrease $a-b$ (-0.0035 to -0.005). The recurrence time increases three times when the effective normal stress change from 10 to 30 MPa (Figure 6d). The recurrence time only increases 40% when $a-b$ decreases from -0.001 to -0.005 (Figure 6b). This is consistent with previous studies, which suggest that SSE duration and recurrence time mostly depend on the effective normal stress (Y. Liu, 2014; Watkins et al., 2015). This is also consistent with analytical solution proposed by Rubin (2008): $T \propto \frac{W}{V_{pl} \mu} \sqrt{a(b-a)}$ (equation (22) in Rubin, 2008, reformatted to be consistent with key parameters discussed here), where T is the recurrence interval of SSEs.

5.2. Testing Hypothesis Two: Effective Normal Stress

The first set of simulations does produce SSE segmentation in certain cases, but these segments have similar duration and interval and are not consistent with observations. Therefore, we run a second set of simulations, allowing parameters to change along strike. For simplicity, we divide the SSE zone into two segments and

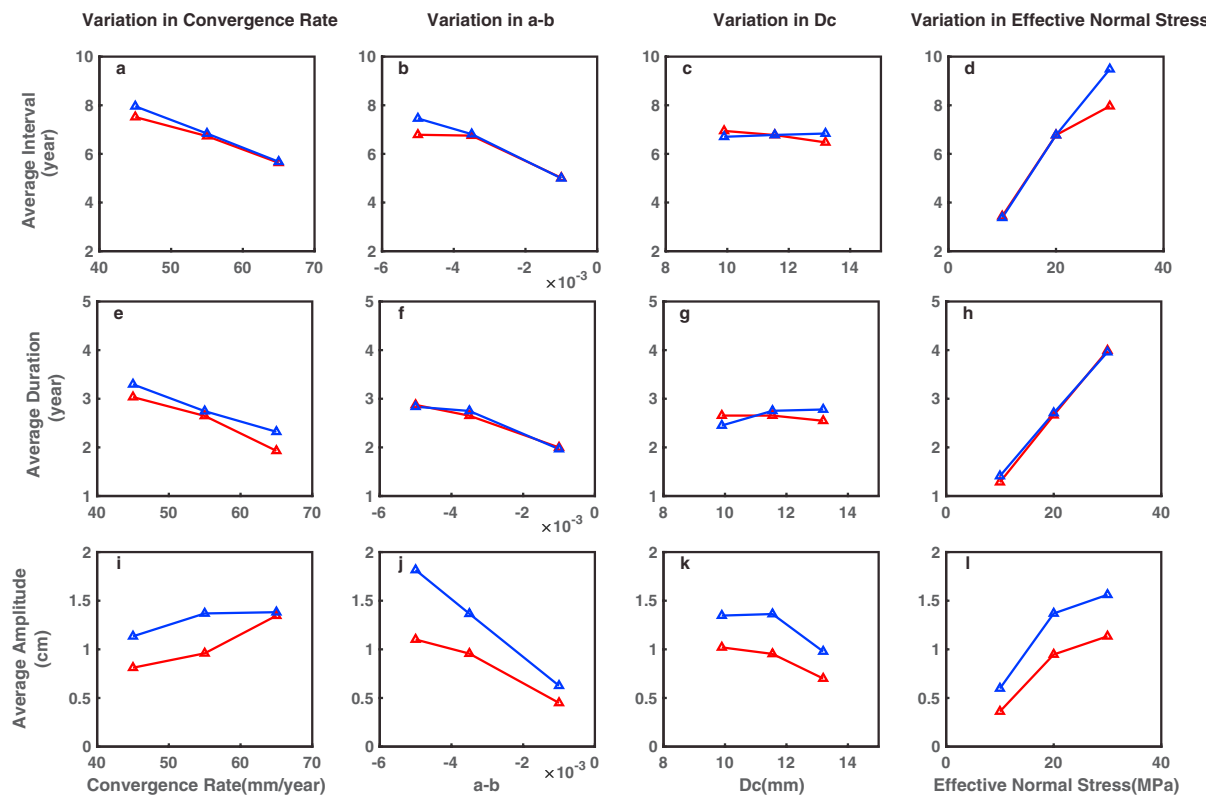


Figure 6. Results from the simulations (Table S3; Test 1–Test 4) of ATW2 are in blue, and those of AC06 are in red. Triangles are the means of actual data points. The influence on the (a–d) mean interval, (e–h) mean duration, and (i–l) mean amplitude of SSEs of variations in convergence rate (V_{pl}), $a-b$, D_c , and effective normal stress ($\bar{\sigma}$).

allow different values of key parameters in these segments. Potentially, large along-strike change of all these key parameters (effective normal stress, W , V_{pl} , μ , and $a-b$) might also contribute to the SSE segmentation. As discussed earlier, the width of the low effective normal stress zone W , the plate subduction rate V_{pl} , and the elastic shear modulus μ are relatively well constrained with no significant along-strike variation. The lab experiments indicate that a and b change with temperature, but there is no 3-D thermal model in this area, so it is not well constrained. On the other hand, the variation of effective normal stress can be linked to well-mapped structure, for example, the Yakutat Plateau. Therefore, we focus on testing the idea that the along-strike variation of effective normal stress can produce the along-strike segmentation of SSEs in south central Alaska.

We run a series of simulations with different values of effective normal stress on the subduction interval at Upper and Lower Cook Inlet, aiming to find the best set of values to reproduce GPS observations. First, our model produces two spatially distinct SSE patches that mimic the observed SSE distributions (Figure 7). Our modeling result supports the hypothesis that a variation in the effective normal stress could explain the along-strike variation of SSEs. Second, the average duration and interval of SSEs at one segment increase with the effective normal stress on the fault interface at the segment (Figure 8). The average duration of SSEs in Lower Cook Inlet increases to 2 years from 1 year when the effective normal stress increases from 10 MPa to 15 MPa. The average duration of SSEs in Upper Cook Inlet increases from 3 to 4 years when the stress increases from 25 to 35 MPa. A combination of 15 MPa stress at Lower Cook Inlet and 30 MPa stress at Upper Cook Inlet can reproduce the observed different duration and interval of the two segments. This is our preferred model (Figures 5c and 5f).

5.3. Interaction Between the Two SSE Segments

Our numerical model allows us to study the interactions between the Lower and Upper Cook Inlet segments. In our preferred model, the two segments rupture independently and regularly (Figure 7). The SSEs in Lower Cook Inlet occur every 7 years, and the SSEs in Upper Cook Inlet rupture about every 11 years. In our

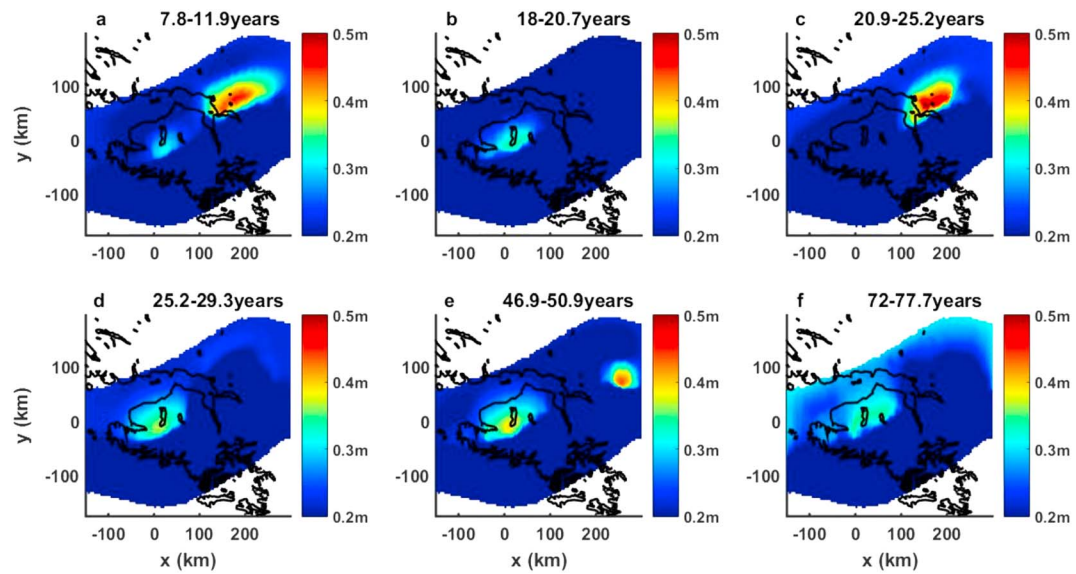


Figure 7. Spatial distribution of several simulated SSEs.

parameter setting, there is no permanent barrier between the two SSE segments. Whether an SSE will rupture to the other side depends on the stress state of the other side. If the other side is close to failure, an SSE from one side will rupture through. However, if the other side just experienced an event and is still early in its own cycle, an SSE from one side will not rupture to the other side. We do not observe any permanent barrier between the two segments. S. Li et al. (2016) found a persistently locked region that separated the two SSE regions based on dense campaign GPS data. It is possible that additional mechanism such as along-strike variation of other parameters that helps to maintain this separation.

5.4. The Migration Speed and the Scaling of SSEs

Fu et al. (2015) studied the spatial-temporal evolution of the 2008–2013 SSE in Upper Cook Inlet by applying a time-dependent Kalman filter slip inversion method to GPS data. The SSE nucleated in the east near the Prince William Sound asperity and then migrated laterally to the west at about 110 km/yr (0.3 km/d). The migration speed is similar to what has been observed for long-term SSEs in southwest Japan (Z. Liu et al., 2010) and Guerrero, Mexico (Radiguet et al., 2011). In our simulation, SSEs migrate both along-strike and along dip at a speed of about 100 km/yr, which is consistent with the GPS observation.

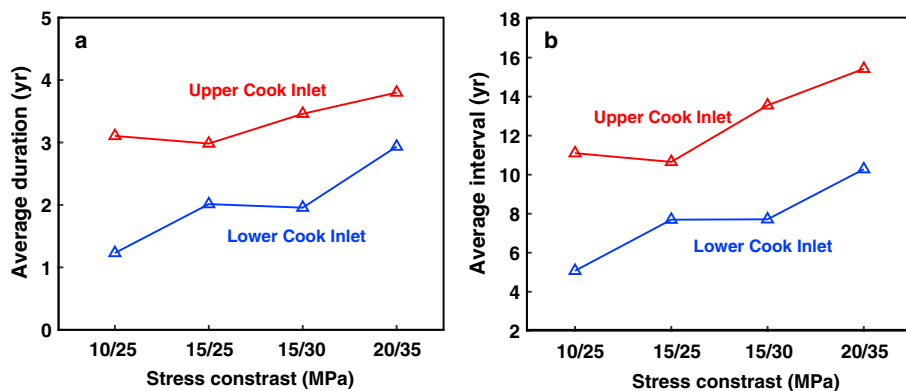


Figure 8. (a) Average duration and (b) interval of SSEs in Upper Cook Inlet and Lower Cook Inlet with different values of effective normal stress. For example, 10/25 means the effective normal stress ($\bar{\sigma}$) is 10 MPa on the fault zone in Lower Cook Inlet and 25 MPa on that in Upper Cook Inlet. The D_c is set to be 10 mm for these simulations.

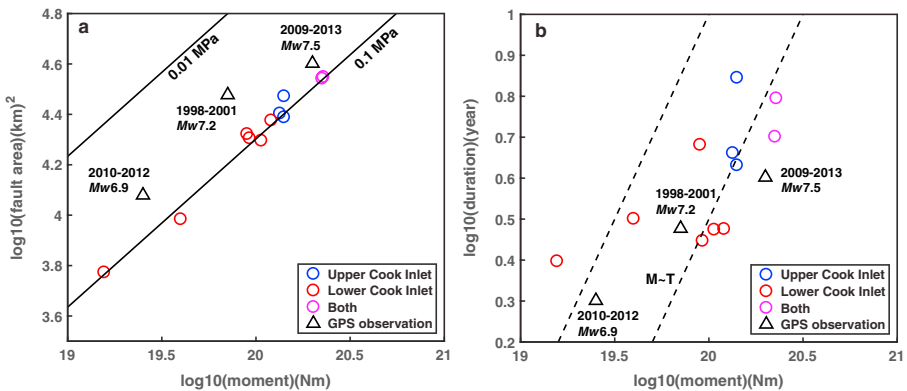


Figure 9. (a) Moment-area scaling relation of both simulated and observed SSEs in south central Alaska. Only the elements with slip greater than twice of the plate rate are accounted in calculating the moment and area. (b) Moment-duration scaling relation of these SSEs.

We quantified the source parameters (equivalent moment, duration, and slip area) of the simulated SSEs in the preferred model (Figure 7). Their scaling relationship is summarized in Figure 9. We also compared them with the observed SSEs in south central Alaska. The modeled SSEs in Upper Cook Inlet are larger in moment and slip area than that in Lower Cook Inlet, but the stress drops are similar at ~ 0.1 MPa (Figure 9a). This is consistent with the stress drop of 0.01–0.1 MPa for SSEs in most subduction zones (H. Gao et al., 2012) and other theoretical and simulation results (D. Li & Liu, 2016; Y. Liu, 2014; Rubin, 2008). These stress drops are 2–3 orders of magnitude lower than regular earthquakes, which may reflect the near-lithostatic pore pressure condition at SSE depth. The simulated SSEs show similar source parameters as observed SSEs in south central Alaska, showing the success of our model to reproduce the observations. The scaling of the moment-duration relationship is more scattered (Figure 9b). There are several SSEs with the same duration but different moment.

6. Discussion

Our results of numerical simulations are consistent with the idea that along-strike variation of effective normal stress creates the along-strike segmentation of SSE in south central Alaska. The contrast in plate buoyance, possibly supplemented by fault zone pore pressure, between the Yakutat Plateau in Upper Cook Inlet and the normal oceanic crust in Lower Cook Inlet is likely the reason of this difference, as elaborated in section 3 and demonstrated in Figure 10. Our work implies that the subducted Yakutat Plateau might have a long-lived effect on the slip behavior of a subduction zone and is very likely a key factor of slow slip event segmentation in south central Alaska.

S. Li et al. (2016) reported an SSE in Lower Cook Inlet that lasted for at least 9 years (1995–2004) (Figure 11). However, at a closer look, as shown in Figure 11, the 9 year long GPS time series could also be interpreted by two small SSEs (5 year and 2 year, respectively) with a quiescent 2 year in between. The onset time of the second small SSE is close to the 2002 M7.9 Denali earthquake, suggesting possible remote dynamic triggering, as best exemplified by the large-scale occurrence of SSEs along the entire Hikurangi margin following the 2016 M7.8 Kaikoura, New Zealand, earthquake (Wallace et al., 2017). Therefore, dynamic stress perturbation could affect SSE behavior if the SSE patch is already at a critical point. Back to the case of Lower Cook Inlet, we acknowledge that the ~ 2 years duration and 7 years interval of SSEs might be only true after 2002. It is difficult to model both the temporal and spatial variations for events spanning 1995 to present with the limited observations. For example, we do not know whether the earlier SSE started in or before 1995, thus impossible to come up with its total duration and cumulative slip. Therefore, we focus our modeling effort for events in Lower Cook Inlet after 2002.

Conflicting results on tremor activity in south central Alaska present an opportunity to test a number of hypotheses associated with tremor triggering. Peterson and Christensen (2009) pioneered tremor studies in Alaska and reported a temporal change of tremor activities associated with the 1998–2001 SSE in Upper Cook Inlet. They documented nonvolcanic tremors in Upper Cook Inlet in the summers of 1999–2001. They found 34 tremors in 1999, 68 in 2000, and 9 in 2001, with most located on the downdip edge of the slip

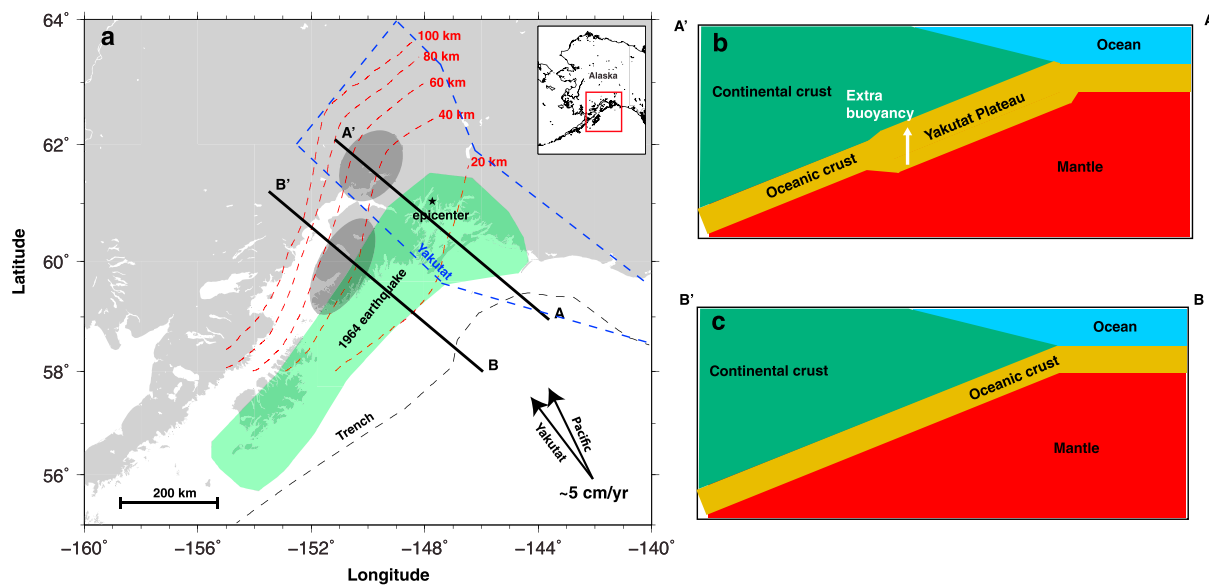


Figure 10. Interpretation of SSE segmentation. (a) Same as in Figure 1, highlighting two profiles. The blue dashed lines indicate the boundary of the subducted Yakutat Plateau (Eberhart-Phillips et al., 2006). (b) Cartoon illustration of cross section along line A–A'. The extent of the Yakutat Plateau provides extra buoyancy that increased the effective normal stress on the subducting interface, which may result in the long-duration SSEs on the east patch. (c) Cartoon illustration of the cross section along line B–B', where the Yakutat Plateau plays no role in the generation of SSEs in Upper Cook Inlet.

region. The dramatic decrease in tremor activity in 2001 is coincident with the end of the 1998–2001 SSE, which suggests a possible temporal correlation between tremors and SSE. This is in contrast to the observations of Wech (2016), who analyzed seismic data between 2007 and 2015 in the same region. He identified tremors also near the downdip edge of the SSE zone but found no temporal variation of tremor intensity that can be associated with the 2009–2012 SSE. One possibility is that the 1998–2001 SSE ruptured at much deeper depth, evidenced by the large displacement at GPS station TLKA during 1998–2001 but not much during the 2009–2013 event. So the deeper rupture of the 1998–2001 SSE created a larger stress change in the tremor area. Another possibility is that long-duration tremors are more sensitive to stress change associated with SSEs. Wech (2016) included all tremors longer than 30 s, whereas

Peterson and Christensen (2009) only looked at tremors longer than 10 min. This is consistent with tremor analysis with only events longer than 3 min between 2005 and 2015; tremor activities increased when an SSE started in 2009 and decreased after the SSE stopped in 2013 (Schultz & Wei, 2016).

Obara and Kato (2016) proposed a synoptic model with a systematic change of SSEs and nonvolcanic tremor behavior along dip: long-term SSEs occur at the downdip end of megaequake and short-term ETS occur next along dip. The SSEs and tremors observed in Upper Cook Inlet in south central Alaska appear to be consistent with this model. Short-term SSEs have been reported in this region but not recorded well due to the small-amplitude and coarse station coverage (Ohta et al., 2007), and tremor activity might be an indication for smaller episodic to semicontinuous aseismic slip.

Our work implies that a structural anomaly will have a long-lived effect on the slip behavior of a subduction zone, including SSE segmentation. It is well known that topographic features such as seamounts, plateaus, ridges, and arcs on the seafloor can modify the mode of subduction as well as the seismic behavior of the thrust (Lay & Kanamori, 1981; Wang & Bilek, 2014, and references therein). Our model results provide another important piece of evidence that

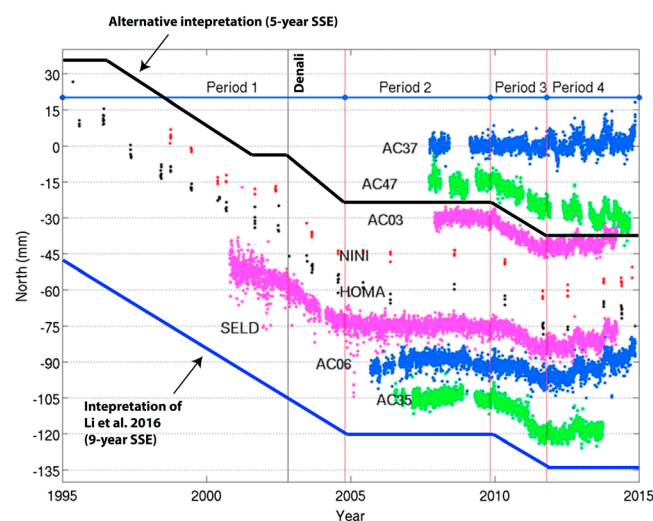


Figure 11. Campaign and continuous GPS data in Lower Cook Inlet (modified from S. Li et al., 2016). The blue solid line is the interpretation by S. Li et al. (2016). The bold black solid line shows an alternative interpretation, in which a change of SSE behavior occurred around the time of the 2002 Denali earthquake.

long-lived geological features, in this case an oceanic plateau, could be a driving force of SSE segmentation through the modification of the normal stress on the fault. Another example is in New Zealand where a subducted seamount is hypothesized to have caused a local reduction in effective stress, due to interface structural relief, which may be a potential factor in promoting shallow SSEs (Bell et al., 2010). The physical conditions (high pore fluid pressure and presence of rough seafloor) that promote SSEs are expected to occur at many other subduction zones (i.e., Saffer & Wallace, 2015), and we expect more research confirming this correlation.

7. Conclusions

GPS and seismic observations indicate strong along-strike segmentation of SSEs in the south central Alaska. Here we reviewed several possible mechanisms that might contribute to the segmentation, such as the along-strike variation of pore pressure related to metamorphic dehydration of the subducting oceanic crust, compositional changes of the upper geological terranes, the slab geometry, and the buoyance of the subducting Yakutat Plateau. We tested two hypotheses (1. slab geometry and 2. effective normal stress) using numerical simulations in the framework of rate-and-state friction with a nonplanar fault geometry. We rejected hypothesis #1 because along-strike variation of slab geometry alone could not reproduce the observed segmentation. Then, we run a set of simulations where we allow the effective normal stress to change along strike. These simulations successfully reproduced key observations such as the interval, duration, magnitude, propagation speed, moment-area scaling of slow slip events, and the observed along-strike segmentation in this region. We suggested that the Yakutat Plateau caused this variation of effective normal stress by either lowering the pore pressure due to less fluids release in Upper Cook Inlet or increasing normal stress due to the extra buoyancy caused by the subducted Yakutat Plateau. We prefer the latter explanation because it is consistent with the level of difference in the effective normal stress and there is very little along-strike variation in V_p/V_s ratio in the fault zone from receiver function analysis. However, we cannot exclude the possibility that the difference in effective normal stress results from along-strike variation of pore pressure due to the uncertainty in V_p/V_s estimation. Our work implies that the subducted Yakutat Plateau might have a long-lived effect on the subduction zone slip behavior and would likely be a key factor of slow slip event segmentation in south central Alaska.

Acknowledgments

We thank reviewers Roland Burgmann and Jeffrey Freymueller for their constructive comments. We thank Editor Yehuda Ben-Zion for handling this manuscript. We thank Magali Billen, Debi Kilb, Samuel Bell, and Nian Wang for helpful discussions. M. Wei and H. Li are supported by the National Science Foundation (OCE 1357433). Y. Kim is supported by the National Research Foundation of Korea (NRF-2014S1A2A2027609) and the Korea Meteorological Administration Research and Development Program (KMIPRA2015-7020). D. Li and Y. Liu are supported by the Natural Science and Engineering Research Council of Canada (NSERC RGPIN 418338-12). The GPS data used in this paper are available on the UNAVCO website (<https://www.unavco.org/data/data.html>); data from numerical modeling of this study are shown in the main text.

References

- Abers, G. A. (2008). Orogenesis from subducting thick crust and evidence from Alaska. In J. G. Freymueller, et al. (Eds.), *Active tectonics and seismic potential of Alaska, American Geophysical Union Geophysical Monograph* (Vol. 179, pp. 337–349). <https://doi.org/10.1029/179GM19>
- Ampuero, J., & Rubin, A. M. (2008). Earthquake nucleation on rate and state faults—Aging and slip laws. *Journal of Geophysical Research*, 113, B01302. <https://doi.org/10.1029/2007JB005082>
- Arrial, P., & Billen, M. I. (2013). Influence of geometry and eclogitization on oceanic plateau subduction. *Earth and Planetary Science Letters*, 363, 34–43. <https://doi.org/10.1016/j.epsl.2012.12.011>
- Audet, P., & Bürgmann, R. (2014). Possible control of subduction zone slow-earthquake periodicity by silica enrichment. *Nature*, 509, 389–392.
- Audet, P., & Kim, Y. (2016). Teleseismic constraints on the geological environment of deep episodic slow earthquakes in subduction zone forearc: A review. *Tectonophysics*, 670, 1–15. <https://doi.org/10.1016/j.tecto.2016.01.005>
- Barnes, D. F., Mariano, J., Morin, R. L., Roberts, C. W., & Jachens, R. C. (1994). Incomplete isostatic gravity map of Alaska. In G. Plafker & H. C. Berg (Eds.), *The Geology of Alaska*, (Vol. G-1). Boulder, CO: The Geological Society of America, The Geology of North America. 1 sheet, scale 1:2,500,000.
- Beeler, N. M., Tullis, T. E., Blanpied, M. L., & Weeks, J. D. (1996). Frictional behavior of large displacement experimental faults. *Journal of Geophysical Research*, 101(B4), 8697–8715. <https://doi.org/10.1029/96JB00411>
- Bell, R., Sutherland, R., Barker, D. H. N., Henrys, S., Bannister, S., Wallace, L., & Beavan, J. (2010). Seismic reflection character of the Hikurangi subduction interface, New Zealand, in the region of repeated Gisborne slow slip events. *Geophysical Journal International*, 180(1), 34–48. <https://doi.org/10.1111/j.1365-246X.2009.04401.x>
- Beroza, G. C., & Ide, S. (2011). Slow earthquakes and nonvolcanic tremor. *Annual Review of Earth and Planetary Sciences*, 39(1), 271–296. <https://doi.org/10.1146/annurev-earth-040809-152531>
- Blanpied, M. L., Marone, C. J., Lockner, D. A., Byerlee, J. D., & King, D. P. (1998). Quantitative measure of the variation in fault rheology due to fluid-rock interactions. *Journal of Geophysical Research*, 103(B5), 9691–9712. <https://doi.org/10.1029/98JB00162>
- Boyarko, D., Brudzinski, M., Porritt, R., Allen, R., & Tréhu, A. (2015). Automated detection and location of tectonic tremor along the entire Cascadia margin from 2005 to 2011. *Earth and Planetary Science Letters*, 430, 160–170. <https://doi.org/10.1016/j.epsl.2015.06.026>
- Brocher, T. M., Fuis, G. S., Fisher, M. A., Plafker, G., Moses, M. J., Taber, J. J., & Christensen, N. I. (1994). Mapping the megathrust beneath the northern Gulf of Alaska using wide-angle seismic data. *Journal of Geophysical Research*, 99(B6), 11,663–11,685. <https://doi.org/10.1029/94JB00111>
- Brudzinski, M. R., & Allen, R. M. (2007). Segmentation in episodic tremor and slip all along Cascadia. *Geology*, 35(10), 907–910. <https://doi.org/10.1130/G23740A.1>
- Christeson, G. L., Gulick, S. P. S., van Avendonk, H. J. A., Worthington, L. L., Reece, R. S., & Pavlis, T. L. (2010). The Yakutat terrane: Dramatic change in crustal thickness across the transition fault. *Geology*, 38(10), 895–898. <https://doi.org/10.1130/G31170.1>

- Christeson, G. L., Van Avendonk, H. J. A., Gulick, S. P. S., Reece, R. S., Pavlis, G. L., & Pavlis, T. L. (2013). Moho interface beneath Yakutat terrane, southern Alaska. *Journal of Geophysical Research: Solid Earth*, 118, 5084–5097. <https://doi.org/10.1002/jgrb.50361>
- Chuang, L., Bostock, M., Wech, A., & Plourde, A. (2017). Plateau subduction, intraslab seismicity, and the Denali (Alaska) volcanic gap. *Geology*, 45(7), 647–650. <https://doi.org/10.1130/G38867.1>
- Cohen, S. C., & Freymueller, J. T. (2004). Crustal deformation in the southcentral Alaska subduction zone. *Advances in Geophysics*, 85, 1–63. <https://doi.org/10.1016/S0065-26870447001-0>
- Colella, H. V., Dieterich, J. H., Richards-Dinger, K., & Rubin, A. M. (2012). Complex characteristics of slow slip events in subduction zones reproduced in multi-cycle simulations. *Geophysical Research Letters*, 39, L20312. <https://doi.org/10.1029/2012GL053276>
- Dieterich, J. H. (1979). Modeling of rock friction: I. Experimental results and constitutive equations. *Journal of Geophysical Research*, 84(B5), 2161–2168. <https://doi.org/10.1029/JB084iB05p02161>
- Dixon, T. H., Yan, J., Rocco, M., Robert, M. C., Nicholas, V., Marino, P., & Gonzalez, V. (2014). Earthquake and tsunami forecasts: Relation of slow slip events to subsequent earthquake rupture. *Proceedings of the National Academy of Sciences of the United States of America*, 111(48), 17039–17044. <https://doi.org/10.1073/pnas.1412299111>
- Doser, D. I., & Veilleux, A. M. (2009). A comprehensive study of the seismicity of the Kenai Peninsula-Cook Inlet Region, south-central Alaska. *Bulletin of the Seismological Society of America*, 99(4), 2208–2222. <https://doi.org/10.1785/0120080251>
- Dragert, G., Wang, K., & James, T. S. (2001). A silent slip event on the deeper Cascadia subduction interface. *Science*, 292(5521), 1525–1528. <https://doi.org/10.1126/science.1060152>
- Eberhart-Phillips, D., Christensen, D. H., Brocher, T. M., Hansen, R., Ruppert, N. A., Haeussler, P. J., & Abers, G. A. (2006). Imaging the transition from Aleutian to Yakutat collision in central Alaska, with local earthquakes and active source data. *Journal of Geophysical Research*, 111, B11303. <https://doi.org/10.1029/2005JB004240>
- Fu, Y., & Freymueller, J. T. (2013). Repeated large slow slip events at the south central Alaska subduction zone. *Earth and Planetary Science Letters*, 375, 303–311. <https://doi.org/10.1016/j.epsl.2013.05.049>
- Fu, Y., Liu, Z., & Freymueller, J. T. (2015). Spatiotemporal variations of the slow slip event between 2008 and 2013 in the southcentral Alaska subduction zone. *Geochemistry, Geophysics, Geosystems*, 16(7), 2450–2461. <https://doi.org/10.1002/2015GC005904>
- Furumoto, A. S. (1965). Analysis of Rayleigh wave, part II. In *Source mechanism study of the Alaska earthquake and tsunami of March 27, 1964, Rep. HIG-65-17* (pp. 31–42). Honolulu: Institute of Geophysics University.
- Gao, H., Schmidt, D. A., & Weldon, R. J. (2012). Scaling relationships of source parameters for slow-slip events. *Bulletin of the Seismological Society of America*, 102(1), 352–360. <https://doi.org/10.1785/0120110096>
- Gao, X., & Wang, K. (2017). Rheological separation of the megathrust seismogenic zone and episodic tremor and slip. *Nature*, 543(7645), 416–419. <https://doi.org/10.1038/nature21389>
- Goldfinger, C., Grijalva, K., Burgmann, R., Morey, A. E., Johnson, J. E., Nelson, C. H., ... Gracia, E. (2008). Late Holocene rupture of the northern San Andreas Fault and possible stress linkage to the Cascadia subduction zone. *Bulletin of the Seismological Society of America*, 98(2), 861–889. <https://doi.org/10.1785/0120060411>
- Hawthorne, J. C., & Rubin, A. M. (2013a). Laterally propagating slow slip events in a rate and state friction model with a velocity-weakening to velocity-strengthening transition. *Journal of Geophysical Research: Solid Earth*, 118, 3785–3808. <https://doi.org/10.1002/jgrb.50261>
- Hawthorne, J. C., & Rubin, A. M. (2013b). Tidal modulation and back-propagating fronts in slow slip events simulated with a velocity-weakening to velocity-strengthening friction law. *Journal of Geophysical Research: Solid Earth*, 118, 1216–1239. <https://doi.org/10.1002/jgrb.50107>
- Hayes, G. P., Wald, D. J., & Johnson, R. L. (2012). Slab1.0: A three-dimensional model of global subduction zone geometries. *Journal of Geophysical Research*, 117, B01302. <https://doi.org/10.1029/2011JB008524>
- He, C., Yao, W., Wang, Z., & Zhou, Y. (2006). Strength and stability of frictional sliding of gabbro gouge at elevated temperatures. *Tectonophysics*, 427(1–4), 217–229. <https://doi.org/10.1016/j.tecto.2006.05.023>
- Hirose, H., & Obara, K. (2010). Recurrence behavior of short-term slow slip and correlated nonvolcanic tremor episodes in western Shikoku, southwest Japan. *Journal of Geophysical Research*, 115, B00A21. <https://doi.org/10.1029/2008JB006050>
- Hyndman, R. D. (2013). Downdip landward limit of Cascadia great earthquake rupture. *Journal of Geophysical Research: Solid Earth*, 118, 5530–5549. <https://doi.org/10.1002/jgrb.50390>
- Ichinose, G., Somerville, P., Thio, H. K., Graves, R., & O'Connell, D. (2007). Rupture process of the 1964 Prince William Sound, Alaska, earthquake from the combined inversion of seismic, tsunami, and geodetic data. *Journal of Geophysical Research*, 112, B07306. <https://doi.org/10.1029/2006JB004728>
- Kim, Y. H., Abers, G. A., Li, J., Christensen, D., Calkins, J., & Rondenay, S. (2014). Alaska megathrust 2: Imaging the megathrust zone and Yakutat/Pacific Plate interface in the Alaska subduction zone. *Journal of Geophysical Research: Solid Earth*, 119, 1924–1941. <https://doi.org/10.1002/2013JB010581>
- Kobayashi, A. (2010). A small scale long-term slow slip occurred in the western Shikoku in 2005 [in Japanese with English figure captions]. *Journal of Seismological Society of Japan (Zisin)*, 63(2), 97–100. <https://doi.org/10.4294/zisin.63.97>
- Kobayashi, A. (2012). Long-term slow slip event around Kochi City from 1978 to 1980 [in Japanese with English abstract and figure captions]. *Journal of Seismological Society of Japan (Zisin)*, 64(2), 63–73. <https://doi.org/10.4294/zisin.64.63>
- Kodaira, S., Iida, T., Kato, A., Park, J.-O., Iwasaki, T., & Kaneda, Y. (2004). High pore fluid pressure may cause silent slip in the Nankai Trough. *Science*, 304(5675), 1295–1298. <https://doi.org/10.1126/science.1096535>
- Lay, T. (2015). The surge of great earthquakes from 2004 to 2014. *Earth and Planetary Science Letters*, 409, 133–146. <https://doi.org/10.1016/j.epsl.2014.10.047>
- Lay, T., & Kanamori, H. (1981). An asperity model of large earthquake sequences. In *Earthquake prediction: An international review*, Maurice Ewing Ser (Vol. 4, pp. 579–592). <https://doi.org/10.1029/ME004p0579>
- Li, D., & Liu, Y. (2016). Spatiotemporal evolution of slow slip events in a non-planar fault model for northern Cascadia subduction zone. *Journal of Geophysical Research: Solid Earth*, 121, 6828–6845. <https://doi.org/10.1002/2016JB012857>
- Li, D., & Liu, Y. (2017). Modeling slow slip segmentation in Cascadia subduction zone constrained by tremor locations and gravity anomalies. *Journal of Geophysical Research: Solid Earth*, 122, 3138–3157. <https://doi.org/10.1002/2016JB013778>
- Li, J., Abers, G. A., Kim, Y. H., & Christensen, D. (2013). Alaska megathrust 1: Seismicity 43 years after the great 1964 Alaska megathrust earthquake. *Journal of Geophysical Research: Solid Earth*, 118, 4861–4871. <https://doi.org/10.1002/jgrb.50358>
- Li, S., Freymueller, J. T., & McCaffrey, R. (2016). Slow slip events and time-dependent variations in locking beneath Lower Cook Inlet of the Alaska-Aleutian subduction zone. *Journal of Geophysical Research: Solid Earth*, 121, 1060–1079. <https://doi.org/10.1002/2015JB012491>
- Liu, Y. (2013). Numerical simulations on megathrust rupture stabilized under strong dilatancy strengthening in slow slip region. *Geophysical Research Letters*, 40, 1311–1316. <https://doi.org/10.1002/grl.50298>

- Liu, Y. (2014). Source scaling relations and along-strike segmentation of slow slip events in a 3-D subduction fault model. *Journal of Geophysical Research: Solid Earth*, 119, 6512–6533. <https://doi.org/10.1002/2014JB011144>
- Liu, Y., McGuire, J. J., & Behn, M. D. (2012). Frictional behavior of oceanic transform faults and its influence on earthquake characteristics. *Journal of Geophysical Research*, 117, B04315. <https://doi.org/10.1029/2011JB009025>
- Liu, Y., & Rice, J. R. (2005). Aseismic slip transients emerge spontaneously in three-dimensional rate and state modeling of subduction earthquake sequences. *Journal of Geophysical Research*, 110, B08307. <https://doi.org/10.1029/2004JB003424>
- Liu, Y., & Rice, J. R. (2007). Spontaneous and triggered aseismic deformation transients in a subduction fault model. *Journal of Geophysical Research*, 112, B09404. <https://doi.org/10.1029/2007JB004930>
- Liu, Y., & Rice, J. R. (2009). Slow slip predictions based on granite and gabbro friction data compared to GPS measurements in northern Cascadia. *Journal of Geophysical Research*, 114, B09407. <https://doi.org/10.1029/2008JB006142>
- Liu, Y., & Rubin, A. M. (2010). Role of fault gouge dilatancy on aseismic deformation transients. *Journal of Geophysical Research*, 115, B10414. <https://doi.org/10.1029/2010JB007522>
- Liu, Z., Owen, S., Dong, D., Lundgren, P., Webb, F., Hetland, E., & Simons, M. (2010). Integration of transient strain events with models of plate coupling and areas of great earthquakes in southwest Japan. *Geophysical Journal International*, 181, 1292–1312. <https://doi.org/10.1111/j.1365-246X.2010.04599.x>
- Matsuzawa, T., Hirose, H., Shibasaki, B., & Obara, K. (2010). Modeling short- and long-term slow slip events in the seismic cycles of large subduction earthquakes. *Journal of Geophysical Research*, 115, B12301. <https://doi.org/10.1029/2010JB007566>
- Matsuzawa, T., Shibasaki, B., Obara, K., & Hirose, H. (2013). Comprehensive model of short- and long-term slow slip events in the Shikoku region of Japan, incorporating a realistic plate configuration. *Geophysical Research Letters*, 40, 5125–5130. <https://doi.org/10.1002/grl.51006>
- Meade, B. J. (2007). Algorithms for the calculation of exact displacements, strains, and stresses for triangular dislocation elements in a uniform elastic half space. *Computers and Geosciences*, 33(8), 1064–1075. <https://doi.org/10.1016/j.cageo.2006.12.003>
- Mitsui, N., & Hirahara, K. (2006). Slow slip events controlled by the slab dip and its lateral change along a trench. *Earth and Planetary Science Letters*, 245(1–2), 344–358. <https://doi.org/10.1016/j.epsl.2006.03.001>
- Nokleberg, W. J., Parfenov, L. M., Monger, J. W. H., Norton, I. O., Khanchuk, A. I., Stone, D. B., ... Fujita, K. (2000). Phanerozoic tectonic evolution of the circum-North Pacific, U.S. *Geol. Surv. Prof. Pap.*, 1626, 122 pp.
- Obara, K. (2002). Nonvolcanic deep tremor associated with subduction in southwest Japan. *Science*, 296(5573), 1679–1681. <https://doi.org/10.1126/science.1070378>
- Obara, K., & Kato, A. (2016). Connecting slow earthquakes to huge earthquakes. *Science*, 353(6296), 253–257. <https://doi.org/10.1126/science.aaf1512>
- Ohta, Y., Freymueller, J. T., Heinsdóttir, S., & Suito, H. (2006). A large slow slip event and the depth of the seismogenic zone in the south central Alaska subduction zone. *Earth and Planetary Science Letters*, 247(1–2), 108–116. <https://doi.org/10.1016/j.epsl.2006.05.013>
- Ohta, Y., Freymueller, J. T., & Miura, S. (2007). The time constant variations of slow slip events in the south Alaska subduction zone. *Eos Trans. AGU*, 88(52), Fall Meet. Suppl., Abstract T21A-0364.
- Okada, Y. (1992). Internal deformation due to shear and tensile faults in a half-space. *Bulletin of Seismological Society of America*, 82(4), 128–140. [https://doi.org/10.1016/0148-9062\(86\)90674-1](https://doi.org/10.1016/0148-9062(86)90674-1)
- Okubo, P. G. (1989). Dynamic rupture modeling with laboratory-derived constitutive relations. *Journal of Geophysical Research*, 94(B9), 12,321–12,335. <https://doi.org/10.1029/JB094iB09p12321>
- Page, R. A., Stephens, C. D., & Lahr, J. C. (1989). Seismicity of the Wrangell and Aleutian Wadati-Benioff zones and the North American plate along the Trans-Alaska Crustal Transect, Chugach Mountains and Copper River basin, southern Alaska. *Journal of Geophysical Research*, 94(B11), 16,059–16,082. <https://doi.org/10.1029/JB094B11p16059>
- Peng, Z., & Gomberg, J. (2010). An integrated perspective of the continuum between earthquakes and slow-slip phenomena. *Nature Geoscience*, 3(9), 599–607. <https://doi.org/10.1038/ngeo940>
- Peterson, C. L., & Christensen, D. H. (2009). Possible relationship between nonvolcanic tremor and the 1998–2001 slow slip event, south central Alaska. *Journal of Geophysical Research*, 114, B06302. <https://doi.org/10.1029/2008JB006096>
- Plafker, G. (1965). Tectonic deformation associated with the 1964 Alaskan earthquake. *Science*, 148(3678), 1675–1687. <https://doi.org/10.1126/science.148.3678.1675>
- Plafker, G., & Berg, H. C. (1994). Overview of the geology and tectonic evolution of Alaska. In G. Plafker & H. C. Berg (Eds.), *The geology of North America, The Geology of Alaska* (Vol. G-1, pp. 989–1021). Boulder, CO: Geological Society of America.
- Pulpan, H., & Frohlich, C. (1985). Geometry of the subducted plate near Kodiak Island and Lower Cook Inlet, Alaska, determined from relocated earthquake hypocenters. *Bulletin of the Seismological Society of America*, 75, 791–810.
- Radiguet, M., Cotton, F., Vergnolle, M., Campillo, M., Valette, B., Kostoglodov, V., & Cotte, N. (2011). Spatial and temporal evolution of a long term slow slip event, the 2006 Guerrero slow slip event. *Geophysical Journal International*, 184(2), 816–828. <https://doi.org/10.1111/j.1365-246X.2010.04866.x>
- Ratchkovski, N. A., & Hansen, R. A. (2002). New evidence for segmentation of the Alaska subduction zone. *Bulletin of the Seismological Society of America*, 92(5), 1754–1765. <https://doi.org/10.1785/0120000269>
- Reber, J. E., Lavier, L. L., & Hayman, N. W. (2015). Experimental demonstration of a semi-brittle origin for crustal strain transients. *Nature Geoscience*, 8(9), 712–715. <https://doi.org/10.1038/NGEO2496>
- Rice, J. R. (1993). Spatiotemporal complexity of slip on a fault. *Journal of Geophysical Research*, 98(B6), 9885–9907. <https://doi.org/10.1029/93JB00191>
- Rogers, G., & Dragert, H. (2003). Episodic tremor and slip on the Cascadia subduction zone: The chatter of silent slip. *Science*, 300(5627), 1942–1943. <https://doi.org/10.1126/science.1084783>
- Rondenay, S., Abers, G. A., & van Keeken, P. E. (2008). Seismic imaging of subduction zone metamorphism. *Geology*, 36(4), 275–278. <https://doi.org/10.1130/G24112A.1>
- Rubin, A. M. (2008). Toward a unified view of tremor and slow slip. AGU Fall Meeting Abstract.
- Rubin, A. M., & Ampuero, J. P. (2005). Earthquake nucleation on (aging) rate and state faults. *Journal of Geophysical Research*, 110, B11312. <https://doi.org/10.1029/2005JB003686>
- Ruina, A. L. (1983). Slip instability and state variable friction laws. *Journal of Geophysical Research*, 88, 10,359–10,370.
- Saffer, D. M., & Wallace, L. M. (2015). The frictional, hydrologic, metamorphic and thermal habitat of shallow slow earthquakes. *Nature Geoscience*, 8(8), 594–600. <https://doi.org/10.1038/ngeo2490>
- Saltus, R. W., Hill, P. L., Connard, G. G., Hudson, T. L., & Barnett, A. (1999). Building a magnetic view of Alaska. *U.S. Geological Survey Open-File Report 99-0418*.

- Schmidt, D. A., & Gao, H. (2010). Source parameters and time-dependent slip distributions of slow slip events on the Cascadia subduction zone from 1998 to 2008. *Journal of Geophysical Research*, 115, B00A18. <https://doi.org/10.1029/2008JB006045>
- Scholz, C. H. (1998). Earthquakes and friction laws. *Nature*, 391(6662), 37–42. <https://doi.org/10.1038/34097>
- Schlitz, W., & Wei, M. (2016). Episodic tremor and slip in south central Alaska. *URI SURFO Technical report*.
- Schwartz, S. Y., & Rokosky, J. M. (2007). Slow slip events and seismic tremor at circum-Pacific subduction zones. *Reviews of Geophysics*, 45, RG3004. <https://doi.org/10.1029/2006RG000208>
- Segall, P., & Rice, J. R. (1995). Dilatancy, compaction, and slip instability of a fluid-infiltrated fault. *Journal of Geophysical Research*, 100(B11), 22,155–22,171. <https://doi.org/10.1029/95JB02403>
- Segall, P., Rubin, A. M., Bradley, A. M., & Rice, J. R. (2010). Dilatant strengthening as a mechanism for slow slip events. *Journal of Geophysical Research*, 115, B12305. <https://doi.org/10.1029/2010JB007449>
- Shelly, D. R., Beroza, G. C., & Ide, S. (2007). Non-volcanic tremor and low-frequency earthquake swarms. *Nature*, 446(7133), 305–307. <https://doi.org/10.1038/nature05666>
- Shelly, D. R., Beroza, G. C., Ide, S., & Nakamura, S. (2006). Low-frequency earthquakes in Shikoku, Japan, and their relationship to episodic tremor and slip. *Nature*, 442(7099), 188–191. <https://doi.org/10.1038/nature04931>
- Shibazaki, B., & Shimamoto, T. (2007). Modelling of short-interval silent slip events in deeper subduction interfaces considering the frictional properties at the unstable—Stable transition regime. *Geophysical Journal International*, 171(1), 191–205. <https://doi.org/10.1111/j.1365-246X.2007.03434.x>
- Skarbek, R. M., & Rempel, A. W. (2016). Dehydration-induced porosity waves and episodic tremor and slip. *Geochemistry, Geophysics, Geosystems*, 17(2), 442–469. <https://doi.org/10.1002/2015GC006155>
- Song, T. R. A., & Simons, M. (2003). Large trench-parallel gravity variations predict seismogenic behavior in subduction zones. *Science*, 301(5633), 630–633. <https://doi.org/10.1126/science.1085557>
- Stephens, C. D., Fogelman, K. A., Lahr, J. C., & Page, R. A. (1984). Wrangell Benioff zone southern Alaska. *Geology*, 12(6), 373–376. [https://doi.org/10.1130/0091-7613\(1984\)12%3C373:WBZSA%3E2.0.CO;2](https://doi.org/10.1130/0091-7613(1984)12%3C373:WBZSA%3E2.0.CO;2)
- Stuart, W. D., Hildenbrand, T. G., & Simpson, R. W. (1997). Stressing of the New Madrid Seismic Zone by a lower crust detachment fault. *Journal of Geophysical Research*, 102(B12), 27,623–27,633. <https://doi.org/10.1029/97JB02716>
- Suito, H., & Freymueller, J. T. (2009). A viscoelastic and afterslip postseismic deformation model for the 1964 Alaska earthquake. *Journal of Geophysical Research*, 114, B11404. <https://doi.org/10.1029/2008JB005954>
- Syracuse, E. M., van Keeken, P. E., & Abers, G. A. (2010). The global range of subduction zone thermal models. *Physics of the Earth and Planetary Interiors*, 183(1–2), 73–90. <https://doi.org/10.1016/j.pepi.2010.02.004>
- Van Wormer, J. D., Davies, J., & Gedney, L. (1974). Seismicity and plate tectonics in south central Alaska. *Bulletin of the Seismological Society of America*, 64, 1467–1475.
- Veenstra, E., Christensen, D. H., Abers, G. A., & Ferris, A. (2006). Crustal thickness variation in south-central Alaska. *Geology*, 34(9), 781–784. <https://doi.org/10.1130/G22615.1>
- Wada, I., & Wang, K. (2009). Common depth of slab-mantle decoupling: Reconciling diversity and uniformity of subduction zones. *Geochemistry, Geophysics, Geosystems*, 10, Q10009. <https://doi.org/10.1029/2009GC002570>
- Waldhauser, F., & Ellsworth, W. L. (2000). A double-difference earthquake location algorithm: Method and application to the northern Hayward fault, California. *Bulletin of the Seismological Society of America*, 90(6), 1353–1368. <https://doi.org/10.1785/0120000006>
- Wallace, L. M., & Beavan, J. (2010). Diverse slow slip behavior at the Hikurangi subduction margin, New Zealand. *Journal of Geophysical Research*, 115, B12402. <https://doi.org/10.1029/2010JB007717>
- Wallace, L. M., Kaneko, Y., Hreinsdóttir, S., Hamling, I., Peng, Z., Bartlow, N., ... Fry, B. (2017). Large-scale dynamic triggering of shallow slow slip enhanced by overlying sedimentary wedge. *Nature Geoscience*, 10(10), 765–770. <https://doi.org/10.1038/ngeo3021>
- Wang, K., & Bilek, S. L. (2014). Invited review paper: Fault creep caused by subduction of rough seafloor relief. *Tectonophysics*, 610(1), 1–24. <https://doi.org/10.1016/j.tecto.2013.11.024>
- Watkins, W. D., Colella, H. V., Brudzinski, M. R., Richards-Dinger, K. B., & Dieterich, J. H. (2015). The role of effective normal stress, frictional properties, and convergence rates in characteristics of simulated slow slip events. *Geophysical Research Letters*, 42, 1061–1067. <https://doi.org/10.1002/2014GL062794>
- Wech, A. G. (2016). Extending Alaska's plate boundary: Tectonic tremor generated by Yakutat subduction. *Geology*, 44(7), 587–590. <https://doi.org/10.1130/G37817.1>
- Weeks, J. D. (1993). Constitutive laws for high-velocity frictional sliding and their influence on stress drop during unstable slip. *Journal of Geophysical Research*, 98(B10), 17,637–17,648. <https://doi.org/10.1029/93JB00356>
- Wei, M., Kaneko, Y., Liu, Y., & McGuire, J. J. (2013). Episodic fault creep events in California controlled by shallow frictional heterogeneity. *Nature Geoscience*, 6(7), 566–570. <https://doi.org/10.1038/ngeo1835>
- Wei, M., McGuire, J. J., & Richardson, E. (2012). A slow slip event in the south central Alaska Subduction Zone and related seismicity anomaly. *Geophysical Research Letters*, 39, L15309. <https://doi.org/10.1029/2012GL052351>
- Wells, R. E., Blakely, R. J., Sugiyama, Y., Scholl, D. W., & Dinterman, P. A. (2003). Basin-centered asperities in great subduction zone earthquakes: A link between slip, subsidence, and subduction erosion? *Journal of Geophysical Research*, 108(B10), 2507. <https://doi.org/10.1029/2002JB002072>
- Worthington, L. L., Van Avendonk, H. J. A., Gulick, S. P. S., Christeson, G. L., & Pavlis, T. L. (2012). Crustal structure of the Yakutat terrane and the evolution of subduction and collision in southern Alaska. *Journal of Geophysical Research*, 117, B01102. <https://doi.org/10.1029/2011JB008493>
- Zhu, L., & Kanamori, H. (2000). Moho depth variation in Southern California from teleseismic receiver functions. *Journal of Geophysical Research*, 105(B2), 2969–2980. <https://doi.org/10.1029/1999JB900322>